nature communications

Article

https://doi.org/10.1038/s41467-025-65150-y

Psilocybin alters visual contextual computations

Received: 14 March 2025

Accepted: 8 October 2025

Published online: 21 November 2025

Check for updates

Marco Aqil[1,2,3] ✉, Gilles de Hollander[4,5], Nina Vreugdenhil[1,2,3], Tomas Knapen[1,2,3,7] & Serge O. Dumoulin[1,2,3,6,7]

Psilocybin alters perception and brain dynamics. Here, we investigate the effects of psilocybin using psychophysics, ultra-high field functional MRI, and computational modeling. We find that psilocybin alters contextual perception in the Ebbinghaus illusion, as well as contextual modulation in cortical responses to visual stimuli. We propose a computational model capable of capturing and linking these changes. Leveraging vision as a beachhead, our findings highlight the alteration of contextual computations as a potential general mechanism underlying psychedelic action.

Psilocybin is a classic psychedelic, i.e. a serotonergic hallucinogen. Previous studies showed that psilocybin alters perception and brain dynamics[1–7]. However, the underlying computational mechanisms remain unclear. We hypothesize that a key effect of psychedelics is the alteration of contextual computations; for example, how a visual stimulus interacts with its surroundings. Such contextual computations are ubiquitous in the brain, and computations first discovered in vision have later been observed in other sensory and cognitive domains[8–11].

Here, we investigated the effects of psilocybin in 5 mg and 10 mg doses with psychophysics, ultra-high-field fMRI, and computational modeling in a randomized, double-blind, placebo-controlled, cross-over design. We explicitly tested whether and how psilocybin alters visual-contextual computations in brain and behavior, and provide a computational model of cortical responses at the single-timecourse level. Our findings highlight the alteration of contextual computations as a potential general and parsimonious computational mechanism underlying the effects of psychedelics on brain, behavior, and subjective experience.

Results

Psilocybin alters contextual perception

To examine the effects of psilocybin on contextual perception, we used the Ebbinghaus illusion[12,13]. In this classic visual illusion, the perceived size of a target stimulus is altered by the presence of a visual context consisting of similar (distractor) stimuli. Previous studies related the Ebbinghaus illusion to anatomical and functional properties of primary visual cortex (V1)[13–15].

Here, participants judged which of two concurrently presented visual stimuli was larger, while maintaining fixation on a central cross, following placebo, 5 mg, and 10 mg psilocybin administration (Fig. 1). In control trials, both stimuli were presented in isolation (Fig. 1a, bottom-right inset). On test trials, one of the two stimuli was presented within a context of larger stimuli (Fig. 1a, top-left inset), making it appear perceptually smaller (the Ebbinghaus illusion).

Psilocybin increased the Ebbinghaus illusion by 39% (5 mg), and 59% (10 mg) relative to placebo (Fig. 1b). Relative to veridical stimulus size, the presence of visual context decreased the perceived stimulus size by 6% (placebo). With psilocybin the perceived stimulus size further decreased by 8.3% (5 mg) and 9.6% (10 mg) (two-sided $p_{Bayesian}$: 0.0245 and 0.0092, respectively) (Fig. 1c).

The change in the Ebbinghaus illusion induced by psilocybin could not be explained by changes in noise or lapses, which were also included in the psychophysical model (Methods, Supplementary Fig. 1). Furthermore, perception in control trials (i.e. stimuli presented without context) was unaltered by psilocybin (Fig. 1a shaded gray and Supplementary Fig. 1), showing that the effect of psilocybin was specific to contextual perception.

This finding demonstrates that the Ebbinghaus illusion can be altered by pharmacological means and suggests the alteration of contextual computations as a potential mechanism underlying the effects of psilocybin on perception.

[1]Spinoza Centre for Neuroimaging, Amsterdam, the Netherlands. [2]Computational Cognitive Neuroscience and Neuroimaging, Netherlands Institute for Neuroscience, Amsterdam, the Netherlands. [3]Experimental and Applied Psychology, Vrije Universiteit Amsterdam, Amsterdam, the Netherlands. [4] Zurich Center for Neuroeconomics, Department of Economics, University of Zurich, Zurich, Switzerland. [5]University Research Priority Program (URPP), Adaptive Brain Circuits in Development and Learning, University of Zurich, Zurich, Switzerland. [6]Experimental Psychology, Utrecht University, Utrecht, the Netherlands. [7]These authors contributed equally: Tomas Knapen, Serge O. Dumoulin. ✉e-mail: m.aqil@spinozacentre.nl

https://doi.org/10.1038/s41467-025-65150-y

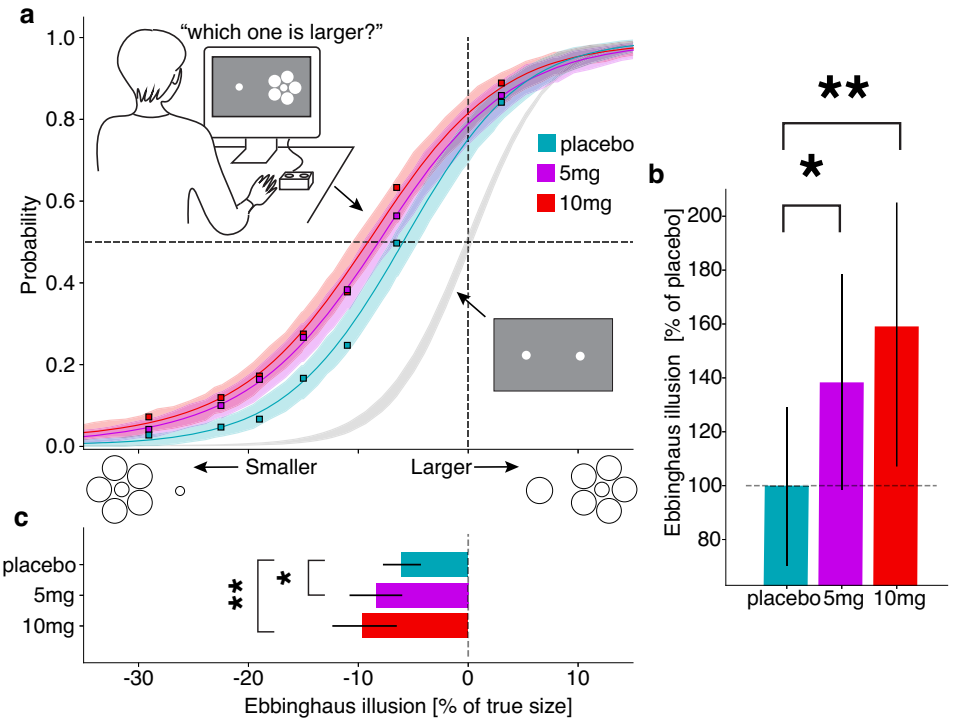

Fig. 1 | Psilocybin alters contextual perception in the Ebbinghaus illusion. **a** Participants judged which one of two concurrently presented stimuli was larger. In control trials, stimuli were presented in isolation (bottom-right inset), and perception was unaltered by psilocybin (shaded gray, Supplementary Fig. 1). In test trials, one stimulus was surrounded by larger stimuli (top-left inset), resulting in a smaller perceived size (Ebbinghaus illusion). Psychometric data for test trials (squares), estimated psychometric curves (colored lines), and 95% highest density intervals for the posterior model predictions (shaded color) are shown for placebo (cyan), 5 mg (magenta), and 10 mg (red) psilocybin doses. **b** Psilocybin increased the Ebbinghaus illusion by 38% (5 mg dose) and 59% (10 mg dose) relative to placebo. **c** Relative to veridical stimulus size, the Ebbinghaus illusion was 6% with placebo administration, 8.3% with 5mg psilocybin (two-sided $p_{Bayesian}$: 0.0245, $n = 18$), and 9.6% with 10mg psilocybin (two-sided $p_{Bayesian}$: 0.0092, $n = 18$). One asterisk indicates $p_{Bayesian} < 0.05$, two $p_{Bayesian} < 0.01$. Error bars represent 95% highest density intervals for model parameter estimates.

Psilocybin alters contextual brain responses

To examine the effects of psilocybin on contextual brain responses, we measured ultra-high field fMRI responses at 7T to a visual stimulus (Fig. 2a), specifically a contrast-defined checkerboard bar sweeping across visual field (Fig. 2b)[16,17]. Participants maintained fixation and performed a color change task at fixation while we recorded eye movements (Fig. 2b, Supplementary Fig. 2). We mapped responses to individual cortical surfaces and identified the visual field maps based on polar angle and eccentricity (Fig. 2c)[18]. Previous studies identified a variety of contextual modulations in brain responses to these visual stimuli, including surround suppression and nonlinear spatial summation[11,17,19,20]. Surround suppression is a particular form of contextual modulation, measurable with various neuroimaging and electrophysiological recording methods[10,11,17,19,21,22].

At the level of single timecourses (example from location indicated with a * in 2c), we found that psilocybin altered contextual brain responses, specifically reducing surround suppression (Fig. 2d, emphasized by black arrows)[17,19]. Averaging bar-sweep responses across visual field maps, we found that psilocybin altered contextual brain responses, specifically reducing surround suppression in early visual field maps V1, V2, and V3 (Fig. 2e–g, emphasized by black arrows). Portions of time courses with significant differences with respect to placebo are indicated with lines below the curves (responses for all visual field maps are shown in Supplementary Fig. 3). Thus, we found that psilocybin altered contextual cortical responses to visual stimuli, specifically reducing surround suppression in early visual field maps.

Computational model captures psilocybin effects

To model cortical responses and capture the alterations induced by psilocybin, we used a recently introduced population receptive field (pRF) model based on divisive normalization (Fig. 3a, Eq (1))[9,11,16,17]. This model captures a variety of contextual modulations in cortical responses, such as surround suppression and nonlinear spatial summation, thanks to local variation in its modulatory parameters, the activation and normalization constants (Fig. 3a and Eq. (1) parameters b and d)[17]. In particular, the activation constant (parameter b in Fig. 3a and Eq. (1)) modulates surround suppression (Fig. 3b).

Identical to Aqil et al.[17], we fit model parameters to maximize variance explained at each cortical location, for each participant, in placebo, 5 mg, and 10 mg doses. We found that individual cortical maps of model variance explained and visual-field eccentricity remained near-identical under placebo and two psilocybin doses (Fig. 3c–h). Furthermore, we found no alterations in model variance explained, activation pRF size, normalization pRF size, and normalization constant in V1 (Fig. 3i–l).

We found a significant, systematic decrease in the model activation constant in early visual field maps V1, V2, and V3 in both psilocybin doses (Fig. 3m), consistent with the reduction in surround suppression observed at the level of single timecourses and entire visual field maps (2d–g). This result could not be explained by potential concurrent changes in noise or hemodynamic response shape, which was also fitted at each cortical location, and verified with a cross-validated approach (Supplementary Figs. 4, 5). The full model parameter estimates for all visual field maps and clusters are reported in Supplementary Fig. 6.

https://doi.org/10.1038/s41467-025-65150-y

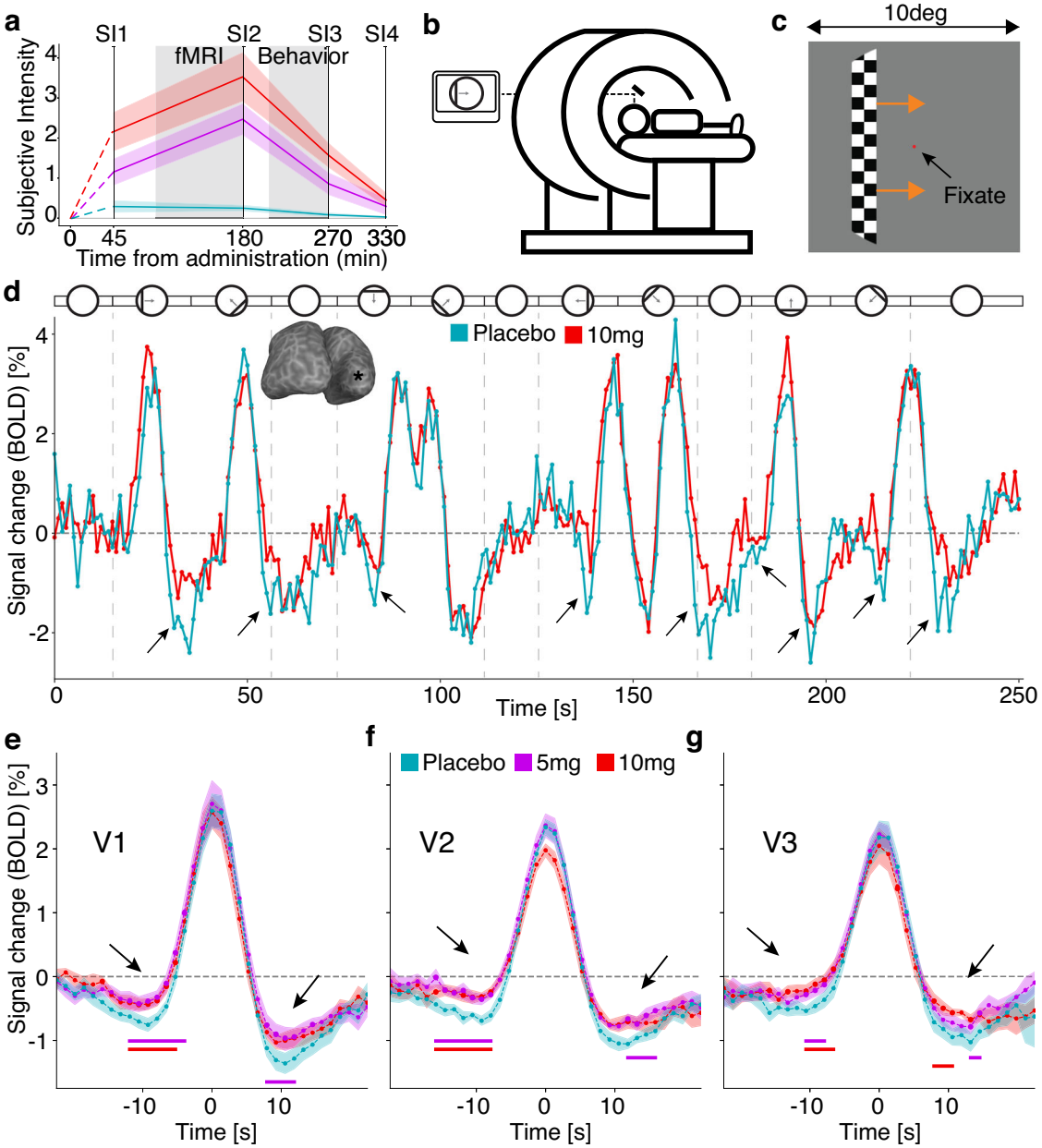

Fig. 2 | Psilocybin alters contextual brain responses, reducing surround suppression in early visual ROIs. a FMRI took place from 90 to 180 min post-administration, and behavioral measures took place from 210 to 270 min post-administration. Time-varying, dose-dependent subjective intensity (SI1-4) confirmed that experiments overlapped with peak and plateau of psilocybin effects (shaded color: ±SEM). **b**, We recorded BOLD responses with 7T fMRI while participants viewed a contrast-defined visual stimulus in individual sessions with placebo, 5mg, and 10 mg psilocybin doses in randomized order. **c** Participants fixated and performed a color change task at fixation while the contrast-defined bar moved through the visual field in eight different directions. We recorded eye movements (Supplementary Fig. 2). **d** Example timecourse from a single participant, single cortical location in V1, in placebo and 10 mg psilocybin doses. On top, a stylized representation of moving-bar stimulus is shown. Asterisk on inset cortical surface indicates the location of the timecourse. Response activation was near-identical in placebo and 10 mg psilocybin doses, but surround suppression, the negative deflections of timecourse flanking the central positive activation peak, was systematically reduced in 10 mg doses (highlighted by arrows). Averaged within visual field maps and across participants (shaded color: ±SEM), responses in **e** V1, **f** V2, and **g** V3 showed significant reduction of surround suppression while activation was not significantly altered. Clusters of consecutive time points with a $p < 0.01$ difference with respect to placebo are indicated with lines below the curves (Fisher permutation test, two-sided, 5000 permutations; cluster corrected with phase-shuffling, 200 folds).

This finding highlights the alteration of contextual computations as a potential mechanism underlying the effects of psilocybin in the human brain, and demonstrates that a computational model can explain the observed changes as a local variation in a specific modulatory parameter (the activation constant, parameter b in Fig. 3a, b and Eq. (1)).

Discussion

Linking brain changes, perception, and subjective experience

In sum, we found that the Ebbinghaus illusion is increased by psilocybin (Fig. 1), while surround suppression is reduced in cortical responses (Fig. 2), an effect captured by a decrease in the activation constant of the normalization model (Fig. 3). We propose that increased Ebbinghaus illusion strength under psilocybin stems from

https://doi.org/10.1038/s41467-025-65150-y

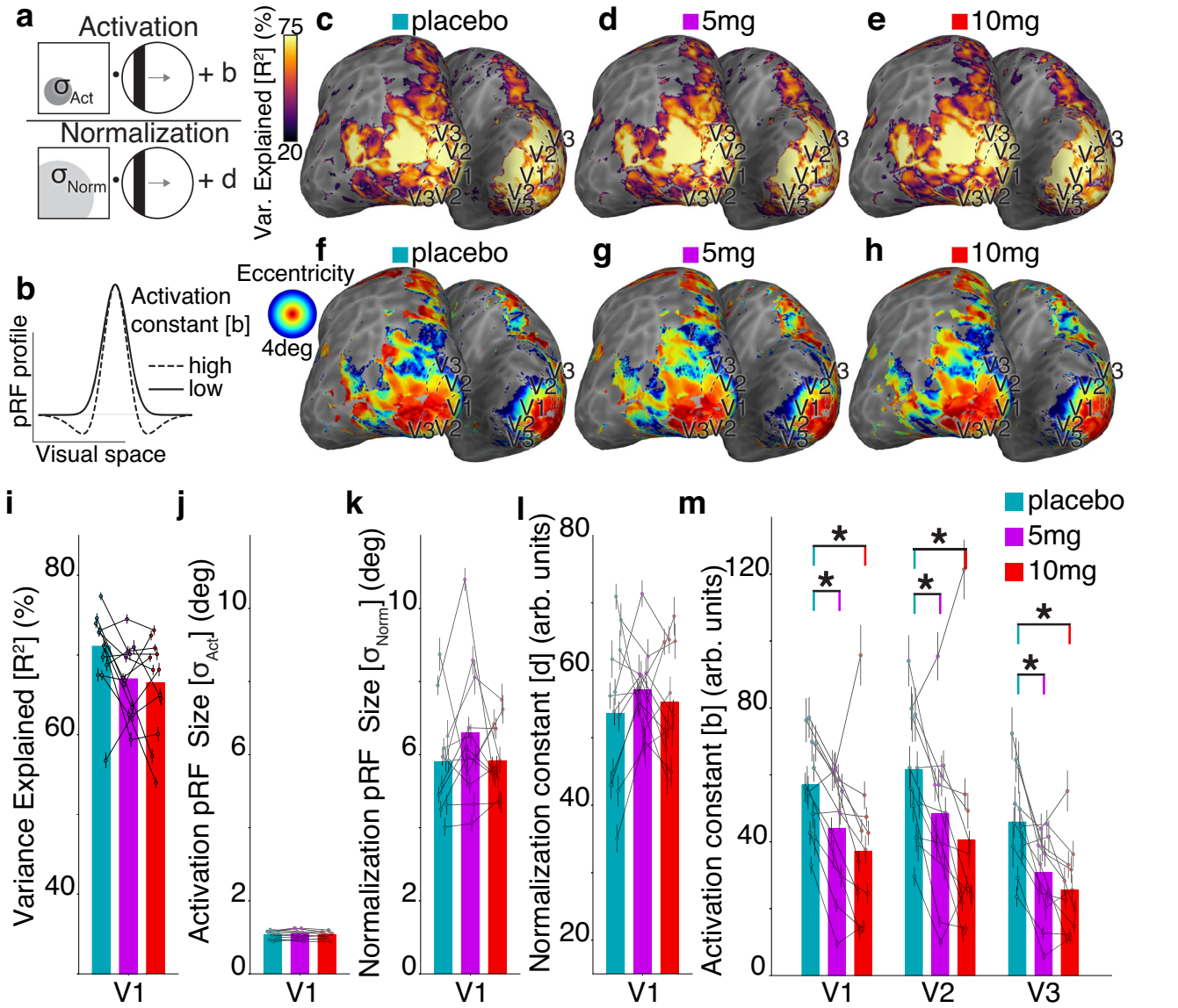

Fig. 3 | Computational model captures psilocybin's effects through a specific parameter. a Schematic of the pRF model based on divisive normalization (Eq. (1)). The model prediction is the ratio of activation and normalization components, convolved with a hemodynamic response function. Activation and normalization terms are derived from the dot-product of a 2D Gaussian in visual space with the stimulus. At each cortical location, the optimal model prediction is obtained by maximizing variance explained (R^2) as a function of the model parameters. **b** The activation constant (parameter b) modulates surround suppression. Higher activation constant increases surround suppression (dashed profile). **c** Example cortical maps of variance explained in placebo, **d** 5 mg, and **e** 10 mg for one participant showing near-identical model fits. **f** Example cortical maps of eccentricity in placebo, **g** 5 mg, and **h** 10 mg for one participant showing the near-identical retinotopic structure. Psilocybin did not significantly alter **i**, variance explained **j**, activation pRF sizes, **k** normalization pRF sizes, nor **l**, the normalization constant in V1. Individual participants are indicated with lines. **m** Psilocybin significantly decreased estimates of the activation constant (parameter b) in early visual field maps (V1-3), consistent with the observation of reduced surround suppression. Asterisks indicate $p < 0.01$ (Fisher permutation test, two-sided, 10^6 permutations, $n = 12$).

reduced cortical surround suppression in early visual cortex. Though we did not hypothesize opposite directions a priori, we have observed similar opposite directions of pRFs and perception under the influence of attention, i.e., where we linked pRF attraction[23] to perceptual repulsion[24]. Previous studies show that Ebbinghaus illusion strength is inversely correlated with V1 surface area[14,25], and that V1 surface area is itself inversely correlated with pRF size[13,15,26]. Thus, individuals with larger V1s, implying greater cortical distance between target and surround representations, experience weaker illusions, likely due to less overlapping and more precise receptive field tuning. Conversely, smaller V1s result in more overlapping pRFs and less precise spatial tuning, leading to stronger illusions. Surround suppression enhances tuning precision[10,27], but psilocybin appears to disrupt this surround suppression, reducing spatial tuning precision and thereby increasing illusion strength. Supporting this notion, we found a significant correlation, albeit limited by sample size, between the psilocybin-induced reduction in V1 surround suppression (as indexed by the DN model activation constant) and the increase in Ebbinghaus illusion strength (Supplementary Fig. 7).

Perceptual precision is determined by multiple distinct mechanisms, such as surround suppression and RF sizes. Our fMRI results suggest that psilocybin specifically alters surround suppression. In line with this result, we only observe differences in the contextual condition of the Ebbinghaus task. A distinct and broader alteration in tuning

precision, for example, via larger pRF sizes, could instead have resulted in flatter psychometric functions in both Ebbinghaus and control conditions. Together, our fMRI and behavioral results consistently suggest that psilocybin elicits a specific alteration of visual-contextual computation in both brain and perception.

Psilocybin, like other classic psychedelics, causes a variety of dose-dependent subjective visual phenomena[28]. We speculate that the observed reduction in surround suppression might be related to these subjective visual phenomena. In an "unsuppressed" state, the visual system would allow increasing amounts of activity, normally quenched by surround suppression, to instead persist and propagate. We found significant correlations between the psilocybin-induced change in V1 estimates of the model activation constant and subjective ratings of classic psychedelic visual phenomena such as "I see geometric patterns" and "I see movement in things that aren't really moving" (Supplementary Fig. 7), while lacking correlations with non-visual questionnaire items (Supplementary Information 8, Supplementary Fig. 9). We remark that these correlations do not survive a full (21-fold) multiple comparison correction, and are limited in power by sample size. Nonetheless, they draw a cautious link between brain and subjective experience.

In this study, we compared the effects of an inert placebo with 5 mg and 10 mg psilocybin doses using a double-blind crossover design. Functional unblinding is an inherent limitation of studies involving psychoactive substances such as psilocybin, given the noticeable subjective effects occurring already at low doses[29]. However, we consider it unlikely that expectation effects or unblinding could explain our results, which pertain to low-level visual computations and are independent of participant choices, beliefs, and expectations. Participants self-assessed confidence in their task performance in psilocybin conditions was lower than in placebo. However, their actual task performance was comparable across all conditions (Supplementary Figs. 1, 2).

FMRI and clinical studies of psilocybin have generally focused on outcomes at high doses (25 mg)[30]. Changes in attentional capabilities may contribute to the effects of psilocybin at high doses, associated with stronger subjective effects and greater potential for impaired task performance and attention. However, for the dose range used in our study (5 mg and 10 mg), we do not find it likely that attentional changes significantly influenced our results. We specifically selected lower doses to minimize those confounds. An attentional impairment elicited by psilocybin likely results in higher lapse rates and shallower psychometric slopes, reduced fixation stability and color change performance during pRF scans. However, neither lapse rates nor slopes differed across doses (Supplementary Fig. 1). Furthermore, fixation stability and performance during pRF scans were also unaltered (Supplementary Fig. 2). Importantly, the dot-color change task in pRF mapping is independent from the actual pRF mapping stimulus, and is mainly intended to encourage participant fixation and wakefulness, alongside explicit eye-tracking. Additionally, the particular results we observed (changes in visual contextual computations, without changes in performance) are unlikely to be explained by variation in attentional capability. Such attentional changes could be expected to have broader effects, e.g. by reducing behavioral task performance, or altering fMRI response amplitudes. Finally, attentional changes could be expected to be more pronounced in the later visual system, while the changes we observe are largest, and occur at lower doses, in the early visual system. In sum, while attentional changes may be a confound or relevant outcome in high-dose psilocybin studies, the available evidence argues against attentional changes underlying the effects of this study.

A common limitation of placebo-controlled studies with psychoactive substances is the potential for results to be confounded by generic effects of altered consciousness. However, we do not find it likely that a generic alteration of consciousness could provide an explanation of our results. If our results simply reflected diminished behavioral performance (e.g., increased noise, lapses and unchanged illusion effects; see Supplementary Fig. 1), or only showed changes in amplitude or a linear scaling of fMRI responses (which could have manifested in response timecourses in Fig. 2e–g), a generic altered state would be a more plausible explanation. Instead, the specificity of our results, which pertain in both fMRI and behavioral domains to visual-contextual alterations, the participants' ability to maintain task performance and fixation at this dose range of psilocybin, and inability of noise or pure hemodynamic changes to explain fMRI signal changes (Supplementary Figs. 4, 5) strongly suggest to us a neuro-computational origin as the most parsimonious explanation.

Here, we found that psilocybin increased the Ebbinghaus illusion by 38% in 5mg dose, and 59% in 10mg dose, which we suggest is due to changes in visual-contextual computations in the early visual cortex. A decision-level cognitive bias elicited by psilocybin could have led participants to more often choose a particular type of stimulus independent of perception, e.g., a decision-making heuristic of picking the isolated circle[31]. We believe this alternative explanation is unlikely. Bayesian accounts predict that stronger biases or heuristics should accompany greater sensory noise, as these typically emerge with increased neural noise as compensatory strategies[32]. Our psychophysical model parameter estimates show no such increase in noise (Supplementary Fig. 1), providing evidence against this interpretation. Furthermore, the alteration in computational model parameters, observed particularly in early visual cortex, is difficult to reconcile with a purely cognitive bias. Considering our fMRI and behavioral results, and prior evidence linking the Ebbinghaus illusion to early visual cortex[14,15], we believe that a change in surround suppression, rather a change in high-level decision-making heuristics, best explains our results. Finally, we find statistically significant correlations between fMRI and behavioral effects (Supplementary Fig. 7) which, albeit limited in power by the small sample size, support a potential link between the two.

Altered contextual processing as a key mechanism of psychedelics

We propose that changes in the model activation constant reflect a broader effect of psychedelics on contextual computations, particularly on surround suppression. Supporting this, a previous psychophysical study in humans found increased perceptual contrast surround suppression with high-dose psilocybin (25 mg)[33]. Using other psychedelic substances (DOI and DMT), a two-photon imaging study in mice reported reduced surround suppression[34], whereas a study using a Gaussian pRF model found larger sizes in V1[35]. Here, we unify these seemingly disparate findings in the context of human spatial vision.

Alterations in contextual computations link our findings to clinical, phenomenological, and neuroscientific evidence. Contextual computations[36], divisive normalization[9], surround suppression[10], and receptive fields[18] are fundamental to cortical responses across sensory and cognitive domains. Contextual factors play a key role in psychedelic experience and therapeutics[5,37]. Psychedelics show promise in the treatment of depression[38], which has been linked to impaired integration of current input with context[36]. Studies in animal models have shown that psychedelics reopen a critical period for contextual reward learning[39]. Thus, our findings suggest that altered contextual computations may drive psychedelic effects in the human brain. We speculate that a simple, widespread computational change across sensory and cognitive domains could explain the diversity and paradoxical nature of psychedelic effects.

In sum, we found that psilocybin alters contextual perception in the Ebbinghaus illusion, contextual modulations in brain responses to visual stimuli, and proposed a computational model to capture and

link these changes. Our findings suggest that altered contextual computations may serve as a general and parsimonious mechanism underlying the effects of psychedelics on brain and behavior.

Methods

Recruitment and exclusion criteria

Participation was solicited via public online means. Interested participants completed an online form, which was used as an initial screening for exclusion criteria. Participants received a small monetary compensation for each completed study session (€35 for preliminary data collection session, and €50 for each experimental session). The exclusion criteria consisted of an age below 21 years, age above 55 years, no prior experience with hallucinogens, previous adverse reactions to hallucinogens, previous adverse responses to MRI, personal or family history of psychiatric or neurological conditions, or ongoing use of medications or recreational drugs. Participants were asked to refrain from the use of recreational drugs in the four weeks leading up to the experiment and between the experimental sessions.

Participants who did not meet any exclusion criteria based on the online questionnaire responses were invited to the Spinoza Centre for further in-person screening. Participants who did not meet any exclusion criteria based on online and in-person screening participated in a preliminary data collection session. During this session, we collected two anatomical scans and one functional scan to ensure that participants had normal fixation ability and eye movement traces, as well as normal or corrected-to-normal visual acuity. Two prospective participants were excluded at this screening stage, before being enrolled in the study, because of the presence of potentially abnormal eye movements (nystagmus). This selection process ensured that all participants were not naive to MRI scanning and to the experimental tasks during their participation in the study.

Participants

Eighteen participants (aged 22–45 years, eight female) were enrolled in the study. All participants had normal or corrected-to-normal visual acuity. All studies were performed with the written informed consent of the participants and were approved by the Medical Ethics Committee (METC) of the Amsterdam University Medical Centre. Data from five participants were excluded from analysis because of the presence of scanner artifacts (coil failures) during one or more of their sessions. Data from one participant were excluded from the analysis due to excessive head motion in one session. A total of twelve participants were included in the final analysis of fMRI data.

Experimental design

The experiment followed a randomized, double-blind, placebo-controlled, crossover design. Each participant underwent three experimental sessions and was administered placebo (25 mg microcrystalline cellulose), 5 mg psilocybin, and 10 mg psilocybin, in random order, at least 2 weeks apart from each other.

We selected experimental timing to ensure that fMRI and behavioral assessments optimally overlapped with the time course of psilocybin effects[40]. Specifically, we conducted fMRI scans from 90 to 180 min post-administration, and collected behavioral measures from 210 to 270 min post-administration. Measures of subjective intensity confirmed that these intervals overlapped with peak and plateau of psilocybin effects (Fig. 2a, Supplementary Fig. 2a).

Previous neuroimaging studies typically used higher doses (up to 25 mg)[6]. Our results demonstrate that intermediate doses of psilocybin are sufficient to alter perception (Fig. 1) and cortical responses (Fig. 2), without significantly impairing fixation ability or performance on simple tasks (Supplementary Fig. 2). Higher doses may impair task performance or fixation, potentially confounding psilocybin's computational effects with noise.

Psychophysical model

In the Ebbinghaus illusion, participants were asked to fixate on a central cross and presented white circles on an isoluminant background for a short interval (0.4 s). After each presentation, they were instructed to report via a button press whether they perceived the right or left circle as larger. In control trials, the two circles were presented in isolation. In test trials, one of the circles was presented surrounded by a set of larger circles. Control and test conditions comprised of 180 trials each, with a constant reference stimulus radius of 0.625, opposite stimulus radii of [0.481, 0.545, 0.580, 0.600, 0.625, 0.650, 0.674, 0.721, 0.812] for the control condition and [0.366, 0.443, 0.484, 0.506, 0.531, 0.556, 0.584, 0.644, 0.770] for the test condition, all expressed in deg of visual angle. We estimated a standard psychophysical model, in which the perception of the two stimulus features (the radius of the reference stimulus r_r and the embedded stimulus r_e) are formally described as samples from two normal distributions:

$$r_r \sim \mathcal{N}(r, \sigma^2), \quad r_e \sim \mathcal{N}(e+\delta, \sigma^2),$$

where r is the actual radius of the reference stimulus and e is the actual radius of the embedded stimulus; σ^2 quantifies the inherent perceptual noise due to sensory processing limitations or neural variability in representing the stimulus radii; δ captures systematic biases in perceiving the radius of the embedded stimulus, potentially driven by contextual effects in the Ebbinghaus illusion. The probability that a participant indicates the reference stimulus is larger than the embedded stimulus can be described by their difference distribution:

$$p(r_r > r_e \mid r, e, \sigma^2, \delta) = \Phi\left(\frac{r-e-\delta}{\sqrt{2}\sigma}\right),$$

where Φ is the standard normal cumulative density function.

To account for lapses, we also estimated the proportion of trials p, on which the participant did not process the stimulus and responded randomly:

$$p(r_r > r_e \mid r, e, \sigma^2, \delta, p) = \frac{1}{2}p + (1-p)\Phi\left(\frac{r-e-\delta}{\sqrt{2}\sigma}\right).$$

The noise parameter σ^2, the bias parameter δ, and the lapse parameter p were estimated in a hierarchical framework using the No U-Turn (NUTS) Hamiltonian MCMC sampler as implemented in `pymc`[41]. The psychometric model was implemented in the Python package `bauer`[42].

For a given parameter θ (e.g., σ^2 or δ), the participant-session-specific parameter of participant p at session t was modeled as:

$$\theta_{p,t} = \mu + \zeta\sigma,$$

where μ is the group mean parameter, σ is the standard deviation of the group distribution, and ζ is an individually determined offset parameter. This offset-based specification of the hierarchical model was chosen to prevent likelihood "funnels" that affect high-dimensional hierarchical models[43].

To estimate the parameters separately for all three dose conditions (placebo/5 mg/10 mg), with and without context, we used a regression approach[44]. A given parameter $\theta_{p,s,g}$ (e.g., δ or σ^2) for observer p on a trial t and dose d was modeled as:

$$\theta_{p,s,g} = \theta_{p,0} + \theta_{p,d}x_{p,d} + \theta_{p,c}x_{p,c} + \theta_{p,d:c}x_{p,d}x_{p,c}.$$

Where $x_{p,c}$ indicated the condition (with or without surrounding circles) of a trial and $x_{p,d}$ the dose (0/5/10 mg). The values of (and the uncertainty in) the estimates of θ could then be used to quantify the relative effect of the different doses, with and without surround. We

used mildly informative priors on all group distribution parameters: For the precision parameter σ:

$$\mu_\nu \sim \mathcal{N}(\text{softplus}^{-1}(1.0), 10.0), \quad \sigma_\nu \sim \text{HalfCauchy}(0.25).$$

Because σ should be bounded between [0, ∞), we estimate it via ν on the unbounded scale and then bring it to the bounded scale using the softplus function to evaluate the likelihood function: $\sigma = \text{softplus}(\nu)$, where $\text{softplus}(x) = \ln(1+e^x)$ is the softplus function and softplus^{-1} is its inverse.)

For the bias parameter δ, we used the following hierarchical parameters

$$\mu_\delta \sim \mathcal{N}(0, 10.0), \quad \sigma_\delta \sim \text{HalfCauchy}(0.25).$$

For the lapse parameter p:

$$p' \sim \mathcal{N}(\text{logit}^{-1}(0.02), 1.0), \quad p' \sim \text{HalfCauchy}(0.25).$$

(Here, p was bounded between 0 and 1 by using the logit function:$\text{p}(x) = \frac{1}{1+e^{-p'}}$, and logit^{-1} is the logistic function. The median of our prior on p was thus 0.02.)

The stimulus set for the Ebbinghaus tasks ranged from 40% smaller to 30% larger than the reference stimulus (the asymmetry in favor of smaller stimuli provided more fine-grained sampling in the perceptual range relevant for the Ebbinghaus illusion) and was determined via earlier pilot trials. The stimulus set included trials with relatively large differences in radius, which allowed us to reliably estimate lapse rates. For those most extreme trials, participants were very close to ceiling performance (max 3.8% error rate for the smallest stimuli and 0.3% for the largest), confirming that it was feasible to estimate the proportion of lapses in our experimental design (Supplementary Fig. 1). Moreover, our Bayesian analysis shows that, at the group level, the posterior estimates of the lapse rates are extremely reliable, with the average 95% CI on lapses being only 1.2% on average over the 6 conditions (3 doses/with or without illusion).

Anatomical MRI scans

T1-weighted and T2-weighted structural MRI data were acquired using a Philips Achieva 7T scanner with an 32-channel Nova Medical head coil, at a resolution of 0.7 mm isotropic. Freesurfer 7.2 recon-all was used to obtain native cortical surface reconstructions for each participant[45]. The software makes use of the T2w image to refine the segmentation obtained from T1w alone, particularly in the exclusion of the sagittal sinus and at the pial surface border. Anatomical segmentations were further refined manually using Freesurfer's software Freeview[45].

Functional MRI scans

Functional MRI data were acquired using a Philips Achieva 7T scanner with an 32-channel Nova Medical head coil. Functional scans were carried out with a 3D EPI sequence, with a repetition time (TR) of 1.32s, and spatial resolution of 1.79 mm isotropic. The first 10 s of recorded data at the beginning of each scan were automatically discarded by the scanner to avoid start-up magnetization transients. Each pRF mapping scan lasted for a total of 255 TRs (approximately 336s). For each participant, in each experimental session, we collected six pRF mapping scans. At the end of each scan, a top-up scan with opposing phase-encoding direction was recorded, to perform susceptibility distortion correction.

Functional MRI data preprocessing

Raw scanner data were converted to nifti using dcm2niix and stored in BIDS format[46]. Thermal denoising was applied using the NORDIC algorithm[47]. Subsequent functional preprocessing steps (susceptibility distortion correction, coregistration, resampling of volumetric data to fsnative surfaces) were performed using fMRIprep v20.7[48,49]. The first 20 principal components of the anatomical and temporal physiological regressors computed by fMRIprep were regressed out using `pybest`[50]. Finally, BOLD timecourses in fsnative surface spaces were converted to percent signal change and highpass filtered to remove drifts using a cosine filter (regressing out the first three components).

Head motion

We estimated motion parameters using MRIQC[51]. We defined excessive motion as a mean frame displacement across scans in a session exceeding one-third of the voxel size (0.6 mm) or a mean of the maximal frame displacement across scans in a session exceeding one voxel size (1.8 mm).

Population receptive field modeling

Population receptive field modeling followed the same procedure as refs. 17,52 and was carried out using dedicated software `prfpy`[53] and `prfpytools`[54]. We used a standard pRF mapping stimulus, a drifting checkerboard bar[16,17]. The stimulus aperture subtended 10deg of visual angle. The checkerboard pattern inside the bar moved parallel to the bar orientation, and the bar itself stepped in the perpendicular direction at every TR (1TR = 1.32 s). Eight bar configurations were presented (two cardinal and two diagonal directions, in two motion directions). The width of the bar subtended 1.25° of visual angle; the bar swept across the stimulus aperture in 20 TR-locked equal-size steps. A period of 15 TRs of mean luminance (0% contrast) was presented every two bar passes. Mean luminance periods of 15 TRs were presented at the beginning and end of each scan. A small fixation dot (0.1°) was presented in the middle of the screen. This fixation dot changed color (from red to green) at semirandom time intervals, and participants reported this change via a button press. The DN model equation was defined as[17]

$$p_{DN}(t) = \frac{a\, G_1 \cdot S + b}{c\, G_2 \cdot S + d} - \frac{b}{d}. \tag{1}$$

The spatial dependence of Gaussian pRFs $G \equiv G(x, y)$ and the spatio-temporal dependence of stimuli $S \equiv S(x, y, t)$ are omitted for brevity, and we denote:

$$G_{1,2} = e^{-\frac{(x-x_0)^2+(y-y_0)^2}{2\sigma_{1,2}^2}}, \quad G_{1,2} \cdot S \equiv \sum_{x,y}(G_{1,2} \circ S),$$

(x_0, y_0) is the response central location in the visual field, σ_1, σ_2 are the sizes of activation and normalization pRFs, a, c their amplitudes, b, d the activation and normalization constants. The neural prediction of the DN model $p_{DN}(t)$ is then convolved with a hemodynamic response function to obtain a prediction of the BOLD fMRI signal at each cortical location. Identically to refs. 17,52, the fitting procedure starts by fitting a Gaussian pRF model, with a grid-search stage followed by an iterative stage, to obtain initial estimates of pRF size and position. These estimates are used as starting parameters for the DN model fit, which also comprises a grid-search and iterative fit stages. First, a grid search is performed vertex-wise for the additional DN model parameters, while keeping the pRF size and position fixed to the Gaussian estimates; next, an iterative fit over all the DN model parameters is performed. Cortical surface visualizations of model parameters (Fig. 3c–h) are obtained with the software package *pycortex*[55].

We focused exclusively on spatial vision. Using simple stimuli that vary in specific dimensions offers significant benefits[56]. These simplified environments make it easier to interpret results and pinpoint how specific computations may be altered. By focusing on spatial vision, we allowed psilocybin's effects on contextual computations to clearly

emerge. This approach could easily be extended to other sensory and cognitive domains (e.g. semantic[57]), where contextual modulations have also been observed[58].

We used a recently developed pRF model based on divisive normalization[9,17]. Other models can also capture surround suppression[19]. However, the DN model uniquely captures a variety of contextual modulations,[17], outperforms other models throughout the human visual system[17], and its parameters correlate with neurotransmitter receptor densities[52]. Since psilocybin could potentially affect other contextual modulations like nonlinear spatial summation, the DN model ensured that the observed changes were specific to surround suppression and not confounded by other potential changes. For these reasons, we concluded the DN model was the best choice to capture psilocybin-induced changes.

Evidence suggests that psilocybin primarily acts through 5-HT2A receptor agonism[1], though 5-HT1A[59,60] and 5-HTT[61] may also play a role. We previously found a correlation between the model's activation constant and 5-HT1A receptor density[52], suggesting 5-HT1A receptor involvement. However, our study was not designed to determine whether a specific receptor or combination drives psilocybin's effects.

Hemodynamic response

The BOLD signal reflects both neuronal and hemodynamic factors, which psilocybin may influence. To account for this, we allowed the HRF shape to vary across cortical locations, participants, and doses, isolating hemodynamic from neuronal changes. Specifically, both grid-search and iterative fit stages of pRF models include a one-parameter hemodynamic response function, computed as a linear combination of the standard SPM-software HRF and of its derivative; the fit parameter represents the coefficient of the HRF derivative. Next, we compared the cross-validated variance explained by models incorporating neuronal, hemodynamic, both, and neither type of change. These analyses confirmed psilocybin induced alterations in cortical responses could not be explained by noise or hemodynamic effects (Supplementary Figs. 4, 5). Notably, a two-photon imaging study in mice, free from hemodynamic confounds, also found reduced neuronal surround suppression, consistent with our findings[34].

Visual regions of interest and clusters

Visual ROIs were defined for each participant on the basis of individual polar angle and eccentricity maps of cortical responses, following refs. 18,62, and similarly to ref. 17.

ROI-wide model parameter estimates

Parameter estimates for each ROI were obtained as the R^2-weighted mean of parameter estimates at each cortical location within the ROI. To prevent edge artifacts or low-signal timecourses from affecting estimates, cortical locations with model $R^2 < 0.3$ or eccentricity outside the bounds of the stimulus range were excluded.

ROI-wide average timecourses

Representative ROI timecourses were obtained as the R^2-weighted mean of timecourses at each cortical location within the ROI, split for each bar-pass, temporally aligned with respect to the pRF position (x_0,y_0) and accounting for HRF delay. To prevent edge artifacts, low-signal timecourses, or timecourses with little or no measurable normalization in the first place from affecting estimates, cortical locations with eccentricity outside the bounds of the stimulus range in any condition, model $R^2 < 0.5$ in any condition, or difference between DN and Gaussian $R^2 < 0.1$ in the placebo condition, were excluded.

At each timepoint, statistical significance of 5 mg and 10 mg differences relative to placebo was computed with a Fisher permutation test across participants (5000 permutations, significance at $p < 0.01$). In order to implement a dedicated cluster correction while also accounting for the temporal autocorrelation of fMRI data, we constructed a null distribution of cluster sizes (consecutive timepoints with $p < 0.01$) through Fourier-domain phase randomization. Specifically, each timecourse of differences relative to placebo, for each dose and participant, was phase-shuffled 200 times. Each shuffled timecourse thus maintained the true size of differences for that dose and participant, the true temporal autocorrelation of fMRI data, and the true alignment of response between doses and placebo, while randomizing the relative temporal location of differences and thus the alignment across participants. For each shuffle, the same Fisher permutation procedure as the original data was applied, in order to create null distributions of cluster sizes. Finally, clusters in the original unshuffled data, for each dose and ROI, were compared to their respective null distributions. Only clusters in the top five percentile of cluster sizes were considered significant. They are indicated by horizontal lines in Fig. 2e–g and Supplementary Fig. 3.

Reporting summary

Further information on research design is available in the Nature Portfolio Reporting Summary linked to this article.

Data availability

The data generated in this study are available under restricted access pursuant to the General Data Protection Regulation (GDPR) and can only be shared based on and subject to the Netherlands Institute for Neuroscience policies. Access can be obtained by contacting the authors (s.dumoulin[@]spinozacentre.nl). Considering the requirements imposed by law and the sensitive nature of personal data, any requests will be addressed on a case-by-case basis, subject to a data usage agreement. Timeframe for response to requests: two weeks.

Code availability

Code is available in dedicated repositories on the open-source platform Zenodo[53,54]. Latest versions can be found on GitHub (https://github.com/VU-Cog-Sci/prfpy, https://github.com/VU-Cog-Sci/prfpytools).

References

1. Halberstadt, A. L. Recent advances in the neuropsychopharmacology of serotonergic hallucinogens. *Behav. brain Res.* **277**, 99–120 (2015).
2. Nichols, D. E. Psychedelics. *Pharmacol. Rev.* **68**, 264–355 (2016).
3. Vollenweider, F. X. & Smallridge, J. W. Classic psychedelic drugs: update on biological mechanisms. *Pharmacopsychiatry* **55**, 121–138 (2022).
4. Van Elk, M. & Yaden, D. B. Pharmacological, neural, and psychological mechanisms underlying psychedelics: a critical review. *Neurosci. Biobehav. Rev.* **140**, 104793 (2022).
5. Carhart-Harris, R. L. & Friston, K. Rebus and the anarchic brain: toward a unified model of the brain action of psychedelics. *Pharmacol. Rev.* **71**, 316–344 (2019).
6. Gill, H. et al. The effects of psilocybin in adults with major depressive disorder and the general population: Findings from neuroimaging studies. *Psychiatry Res.* **313**, 114577 (2022).
7. Siegel, J. S. et al. Psilocybin desynchronizes the human brain. *Nature* **632**, 131–138 (2024).
8. Wandell, B.A. *Foundations of Vision* (Sinauer Associates, 1995).
9. Carandini, M. & Heeger, D. J. Normalization as a canonical neural computation. *Nat. Rev. Neurosci.* **13**, 51–62 (2012).
10. Angelucci, A. et al. Circuits and mechanisms for surround modulation in visual cortex. *Annu. Rev. Neurosci.* **40**, 425–451 (2017).
11. Dumoulin, S. O. & Knapen, T. How visual cortical organization is altered by ophthalmologic and neurologic disorders. *Annu. Rev. Vis. Sci.* **4**, 357–379 (2018).
12. Ebbinghaus, H. *Grundzü*ge der Psychologie v. 1, 1911. (Veit) Vol. 1, (1911).

13. Kirsch, W. & Kunde, W. On the origin of the Ebbinghaus illusion: the role of figural extent and spatial frequency of stimuli. *Vis. Res.* **188**, 193–201 (2021).
14. Schwarzkopf, D. S., Song, C. & Rees, G. The surface area of human v1 predicts the subjective experience of object size. *Nat. Neurosci.* **14**, 28–30 (2011).
15. Song, C., Schwarzkopf, D. S., Kanai, R. & Rees, G. Neural population tuning links visual cortical anatomy to human visual perception. *Neuron* **85**, 641–656 (2015).
16. Dumoulin, S. O. & Wandell, B. A. Population receptive field estimates in human visual cortex. *Neuroimage* **39**, 647–660 (2008).
17. Aqil, M., Knapen, T. & Dumoulin, S. O. Divisive normalization unifies disparate response signatures throughout the human visual hierarchy. *Proc. Natl Acad. Sci.* **118**, e2108713118 (2021).
18. Wandell, B. A., Dumoulin, S. O. & Brewer, A. A. Visual field maps in human cortex. *Neuron* **56**, 366–383 (2007).
19. Zuiderbaan, W., Harvey, B. M. & Dumoulin, S. O. Modeling center–surround configurations in population receptive fields using fmri. *J. Vis.* **12**, 10–10 (2012).
20. Kay, K. N., Winawer, J., Mezer, A. & Wandell, B. A. Compressive spatial summation in human visual cortex. *J. Neurophysiol.* **110**, 481–494 (2013).
21. Klink, P. C., Chen, X., Vanduffel, W. & Roelfsema, P. R. Population receptive fields in nonhuman primates from whole-brain fMRI and large-scale neurophysiology in visual cortex. *Elife* **10**, e67304 (2021).
22. Harvey, B. M. et al. Frequency specific spatial interactions in human electrocorticography: V1 alpha oscillations reflect surround suppression. *Neuroimage* **65**, 424–432 (2013).
23. Klein, B. P., Harvey, B. M. & Dumoulin, S. O. Attraction of position preference by spatial attention throughout human visual cortex. *Neuron* **84**, 227–237 (2014).
24. Klein, B. P., Paffen, C. L., Te Pas, S. F. & Dumoulin, S. O. Predicting bias in perceived position using attention field models. *J. Vis.* **16**, 15–15 (2016).
25. Schwarzkopf, D. S. & Rees, G. Subjective size perception depends on central visual cortical magnification in human v1. *PloS one* **8**, e60550 (2013).
26. Harvey, B. M. & Dumoulin, S. O. The relationship between cortical magnification factor and population receptive field size in human visual cortex: constancies in cortical architecture. *J. Neurosci.* **31**, 13604–13612 (2011).
27. Barlow, H.B. et al. Possible principles underlying the transformation of sensory messages. *Sens. Commun.* **1**, 217–233 (1961).
28. Preller, K.H. & Vollenweider, F.X. Phenomenology, structure, and dynamic of psychedelic states. *Behav. Neurobiol. Psychedelic Drugs*, 221–256 (2016).
29. Hirschfeld, T. & Schmidt, T. T. Dose–response relationships of psilocybin-induced subjective experiences in humans. *J. Psychopharmacol.* **35**, 384–397 (2021).
30. Beneš, M., Páleníček, T. & Horáček, J. What fMRI studies say about the nature of the psychedelic effect: a scoping review. *Front. Neurosci.* **19**, 1606798 (2025).
31. Manning, C., Morgan, M. J., Allen, C. T. & Pellicano, E. Susceptibility to Ebbinghaus and müller-lyer illusions in autistic children: a comparison of three different methods. *Mol. Autism* **8**, 16 (2017).
32. Ma, W.J., Kording, K.P. & Goldreich, D. *Bayesian Models of Perception and Action: An Introduction* (MIT Press, 2023).
33. Swanson, L. R. et al. Enhanced visual contrast suppression during peak psilocybin effects: psychophysical results from a pilot randomized controlled trial. *J. Vis.* **24**, 5–5 (2024).
34. Michaiel, A. M., Parker, P. R. & Niell, C. M. A hallucinogenic serotonin-2a receptor agonist reduces visual response gain and alters temporal dynamics in mouse v1. *Cell Rep.* **26**, 3475–3483 (2019).
35. Pais, M. L. et al. Rapid effects of tryptamine psychedelics on perceptual distortions and early visual cortical population receptive fields. *NeuroImage* **297**, 120718 (2024).
36. Northoff, G. & Mushiake, H. Why context matters? Divisive normalization and canonical microcircuits in psychiatric disorders. *Neurosci. Res.* **156**, 130–140 (2019).
37. Carhart-Harris, R. L. et al. Psychedelics and the essential importance of context. *J. Psychopharmacol.* **32**, 725–731 (2018).
38. Muttoni, S., Ardissino, M. & John, C. Classical psychedelics for the treatment of depression and anxiety: a systematic review. *J. Affect. Disord.* **258**, 11–24 (2019).
39. Nardou, R. et al. Psychedelics reopen the social reward learning critical period. *Nature* **618**, 790–798 (2023).
40. Carbonaro, T. M., Johnson, M. W., Hurwitz, E. & Griffiths, R. R. Double-blind comparison of the two hallucinogens psilocybin and dextromethorphan: similarities and differences in subjective experiences. *Psychopharmacology* **235**, 521–534 (2018).
41. PyMC-Devs, Pymc *Zenodo* https://doi.org/10.5281/zenodo.14611282 (2025).
42. de Hollander, G., Renkert, M.F. & Ruff, C.C. Bauer: Bayesian estimation of perceptual, numerical and risky judgements *Software* (2024).
43. Betancourt, M. J. & Girolami, M. Hamiltonian Monte Carlo for hierarchical models. *Curr. Trends Bayesian Methodol. Appl.* **79**, 2–4 (2015).
44. Wiecki, T. V., Sofer, I. & Frank, M. J. HDDM: hierarchical Bayesian estimation of the drift-diffusion model in Python. *Front. Neuroinform.* **7**, 14 (2013).
45. Fischl, B. Freesurfer. *Neuroimage* **62**, 774–781 (2012).
46. Gorgolewski, K. J. A format for organizing and describing outputs of neuroimaging experiments. *Sci. Data* **3**, 1–9 (2016).
47. Vizioli, L. et al. Lowering the thermal noise barrier in functional brain mapping with magnetic resonance imaging. *Nat. Commun.* **12**, 5181 (2021).
48. Esteban, O. et al. fMRIPrep: a robust preprocessing pipeline for functional MRI. *Nat. Methods* (2018).
49. Esteban, O. et al. fmriprep. *Software* (2018).
50. Snoek, L., Ecasimiro, Lindh, D. & Knapen, T., lukassnoek/pybest: release with Zenodo. https://doi.org/10.5281/zenodo.10837111 (2024).
51. Esteban, O. et al. Mriqc: Advancing the automatic prediction of image quality in mri from unseen sites. *PloS one* **12**, e0184661 (2017).
52. Aqil, M., Knapen, T. & Dumoulin, S. O. Computational model links normalization to chemoarchitecture in the human visual system. *Sci. Adv.* **10**, eadj6102 (2024).
53. Aqil, M., Knapen, T. Prfpy: a Python package to simulate and fit population receptive field models to time series data. (v0.1.0-alpha). *Zenodo*. https://doi.org/10.5281/zenodo.10201022 (2023).
54. Aqil, M., Prfpytools: a Python package for analysis and visualization of population receptive field models. (v0.1.0-alpha). *Zenodo*. https://doi.org/10.5281/zenodo.10209657. (2023).
55. Gao, J. S., Huth, A. G., Lescroart, M. D. & Gallant, J. L. Pycortex: an interactive surface visualizer for fMRI. *Front. Neuroinform.* **9**, 23 (2015).
56. Rust, N. C. & Movshon, J. A. In praise of artifice. *Nat. Neurosci.* **8**, 1647–1650 (2005).
57. Huth, A. G., De Heer, W. A., Griffiths, T. L., Theunissen, F. E. & Gallant, J. L. Natural speech reveals the semantic maps that tile human cerebral cortex. *Nature* **532**, 453–458 (2016).
58. Deniz, F., Tseng, C., Wehbe, L., la Tour, T. D. & Gallant, J. L. Semantic representations during language comprehension are affected by context. *J. Neurosci.* **43**, 3144–3158 (2023).
59. Pokorny, T., Preller, K. H., Kraehenmann, R. & Vollenweider, F. X. Modulatory effect of the 5-ht1a agonist buspirone and the mixed non-hallucinogenic 5-ht1a/2a agonist ergotamine on psilocybin-induced psychedelic experience. *Eur. Neuropsychopharmacol.* **26**, 756–766 (2016).

60. Conn, K. et al. Psilocybin restrains activity-based anorexia in female rats by enhancing cognitive flexibility: contributions from 5-ht1a and 5-ht2a receptor mechanisms. *Mol. Psychiatry* **29**, 3291–3304 (2024).
61. Gattuso, J. J., Wilson, C., Li, S., Hannan, A. J. & Renoir, T. Mice lacking the serotonin transporter do not respond to the behavioural effects of psilocybin. *Eur. J. Pharmacol.* **a**, 177304 (2025).
62. Wandell, B. A., Brewer, A. A. & Dougherty, R. F. Visual field map clusters in human cortex. *Philos. Trans. R. Soc. B: Biol. Sci.* **360**, 693–707 (2005).

Acknowledgements

This research was funded by the Dutch Research Council (NWO) Vici grant 016.Vici.185.050 to S.D. The psilocybin used in this study was provided by Usona Institute. The authors thank the participants for their dedication and support of the study. We also thank Jurjen Heij for support with preprocessing pipelines, Tom Pelletreau-Duris for support in data analysis, and Leon Behle for support in stimulus design and testing.

Author contributions

Conceptualization: M.A., T.K., S.D. Methodology: M.A., G.H., N.V., T.K., S.D. Investigation: M.A., G.H., N.V., T.K., S.D. Visualization: M.A., G.H., N.V. Supervision: T.K., S.D. Writing, original draft: M.A. Writing, review & editing: M.A., G.H., N.V., T.K., S.D. Funding acquisition: S.D.

Competing interests

The authors declare no competing interests.

Additional information

Supplementary information The online version contains supplementary material available at https://doi.org/10.1038/s41467-025-65150-y.

Correspondence and requests for materials should be addressed to Marco Aqil.

Peer review information *Nature Communications* thanks Tessa Dekker, and the other anonymous reviewer(s) for their contribution to the peer review of this work. A peer review file is available.